

A comparison of two wavefield extrapolators: PSPI plus correction verses an efficient Fourier operator

Robert J. Ferguson, Department of Geological Sciences, University of Texas, Austin, and Gary F. Margrave, University of Calgary

SUMMARY

To reduce the cost of migration and modeling, and to relate cost to accuracy, two efficient operators are derived from a general expression for one-way wavefield extrapolation. One operator desamples the input velocity model so that the number of significant values in the extrapolation matrix is reduced, and an efficient implementation is realized. The resulting computational cost is proportional to $mnMN \log_2 MN$, where M and N are the dimensions of the seismic data volume, and m and n are the dimensions of the desampled velocity model. The second operator is based on reducing the number of unique velocities in the model. This results in an extrapolation method similar to PSPI plus correction. The cost of applying this operator is proportional to $pMN \log_2 MN$, where p is the number of unique velocities.

Using the SEG/EAGE Salt model and the IFP Marmousi model, the two operators are compared. For Marmousi, where velocity variation is blocky, the method based on reducing the number of unique velocities returns the greater accuracy for equivalent cost. For the Salt model, variation above and below the salt is smooth, the operator based on desampling the velocity field is more accurate for equivalent cost. At the level of the salt, however, the reduced method returns greater accuracy.

INTRODUCTION

The one-way extrapolation operators that are the subject of this abstract arise from an approximate solution to the wave equation. A one-way operator is constructed with respect to a preferred direction of collimation such that reflections caused by the component of the velocity gradient in the direction of collimation are suppressed. Usually the vertical (z) direction is chosen as the direction of collimation. The solution is approximate in that the lateral variation in elastic parameters is assumed to be weak such that the propagating wavefield doesn't generate other scattered wavefields. One-way operators tend to be faster than the two-way operators and slower than the direct-inverse methods. Also, they don't generate spurious events wherever contrasts in elastic parameters are found, and they naturally allow multiple wave arrivals at single points. In strongly heterogeneous media, however, accuracy is lost for paths that deviate by large angles from the direction of collimation.

Two operators will be derived directly from the Fourier integral operator of wavefield extrapolation. Part of this derivation is identical to the development of the phase-screen operators (Wu and Huang, 1992; Le Rousseau and de Hoop, 2001) with the departure that a stationary, or space invariant, background velocity is not imposed during the derivation.

The focusing term is then modified using two alternative approaches to significantly reduce the cost of application. One approach results in the familiar 'PSPI plus correction' scheme where the phase-shift-plus-interpolation (PSPI) method (Gazdag and Squazzerro, 1984) is combined with a differential thin-lens term from the phase-screen method (Wu and Huang, 1992). When the focusing term is parameterized with the complete model, the result is identical to that of the Fourier integral operator. For a single reference velocity, the result is identical to the phase-screen operator. Parameterization intermediate to these extremes results in operators that balance accuracy and computational efficiency.

The second approach reduces computational cost by smoothing the velocity model laterally. When the resulting operator is applied entirely in the Fourier domain there are fewer nonzero terms, and most

of these are grouped conveniently around the zero wavenumber. Computational efficiency is gained by computing and applying only those non-zero elements. For an all pass smoother, the effective operator is identical to the Fourier integral operator. For a filter that passes only D.C., the effective operator is identical to the phase-screen operator.

For comparison, a simple expression is derived that relates error in the input velocity model and focusing error. This gives a relationship between cost and accuracy with which to evaluate operators, and provides a criteria to tailor operator selection to velocity model as a function of accuracy and computational cost.

METHODOLOGY

Each geophone in a seismic array has a position defined by three orthogonal axes x_1 , x_2 , and z . Two of them, x_1 and x_2 represented in short by \mathbf{x} , define a plane normal to the approximate direction of the Earth's gravity near the center of the geophone array. Orthogonal to \mathbf{x} , axis z represents depth. We will represent the seismic waves recorded in the geophone array by $\Psi(\mathbf{x}, z, t)$, where t is an axis representing the passage of time since excitation of the source. Fourier transform of Ψ is

$$\psi(\mathbf{x}, z, \omega) = \int \Psi(\mathbf{x}, z, t) e^{-i\omega t} dt, \quad (1)$$

where ω is temporal frequency.

Extrapolation of ψ from z at the surface to $z + \Delta z$ in the subsurface can be computed using a Fourier integral operator.

$$\psi(\mathbf{x}, z + \Delta z, \omega) = \frac{1}{(2\pi)^2} \int \phi(\mathbf{k}, z, \omega) e^{i\Delta z k_z(v(\mathbf{x}), \mathbf{k}, \omega) + i\mathbf{k} \cdot \mathbf{x}} d\mathbf{k}, \quad (2)$$

where \mathbf{k} are wavenumbers corresponding to spatial coordinates \mathbf{x}

$$k_z(v(\mathbf{x}), \mathbf{k}, \omega) = \begin{cases} \sqrt{\left(\frac{\omega}{v(\mathbf{x})}\right)^2 - \mathbf{k} \cdot \mathbf{k}} & \text{if } \left(\frac{\omega}{v(\mathbf{x})}\right)^2 \geq \mathbf{k} \cdot \mathbf{k}; \\ i \left| \sqrt{\left(\frac{\omega}{v(\mathbf{x})}\right)^2 - \mathbf{k} \cdot \mathbf{k}} \right| & \text{if } \left(\frac{\omega}{v(\mathbf{x})}\right)^2 \leq \mathbf{k} \cdot \mathbf{k}. \end{cases} \quad (3)$$

is the wavenumber corresponding to depth, and ϕ is the 2D Fourier transform of the monochromatic wavefield obtained at surface (\mathbf{x}, z)

$$\phi(\mathbf{k}, z, \omega) = \frac{1}{(2\pi)^2} \int \psi(\mathbf{x}, z, \omega) e^{i\mathbf{k} \cdot \mathbf{x}} d\mathbf{x}. \quad (4)$$

Complex values of k_z correspond to the evanescent region where reflection energy is absent. In equation (3), we force complex values of k_z to be positive complex so that the resulting phase term $i\Delta z k_z$ in equation (2) is real valued and negative. The result is that evanescent energy is forced to decrease exponentially.

Because the domain change in equation (2) is not strictly a Fourier transform, the fast Fourier transform algorithm cannot be used directly so the computational effort required for extrapolation is proportional to $MN[M + N]$, where M and N are the dimensions of the recording aperture.

Clearly, approximate operators that can be optimized for accuracy and cost are required. Introduce a background velocity $\tilde{v}(x) \neq v(x)$ into equation (3) so that

$$k_z(v(\mathbf{x}), \mathbf{k}, \omega) = k_z(\tilde{v}(\mathbf{x}), \mathbf{k}, \omega) \sqrt{1 + \frac{\left(\frac{\omega}{v(\mathbf{x})}\right)^2 - \left(\frac{\omega}{\tilde{v}(\mathbf{x})}\right)^2}{k_z^2(\tilde{v}(\mathbf{x}), \mathbf{k}, \omega)}}, \quad (5)$$

The first-order expansion of equation (5) is

$$k_z(v(\mathbf{x}), \mathbf{k}, \omega) \approx k_z(\tilde{v}(\mathbf{x}), \mathbf{k}, \omega) + \frac{1}{2k_z(v(\mathbf{x}), \mathbf{k}, \omega)} \times \left[\left(\frac{\omega}{v(\mathbf{x})} \right)^2 - \left(\frac{\omega}{\tilde{v}(\mathbf{x})} \right)^2 \right] \quad (6)$$

From the second term of equation (6), expand $k_z(\tilde{v})$ about $\mathbf{k} = 0$ and equation (2) becomes

$$\Psi_a(\mathbf{x}, z + \Delta z, \omega) \approx \tilde{\Psi}(\mathbf{x}, z, \omega) e^{i\Delta z \frac{\tilde{v}}{\omega} \left[\left(\frac{\omega}{v(\mathbf{x})} \right)^2 - \left(\frac{\omega}{\tilde{v}(\mathbf{x})} \right)^2 \right]}, \quad (7)$$

where subscript a in Ψ_a indicates an approximation to the result from the full Fourier integral operator of equation (2), and

$$\tilde{\Psi}(\mathbf{x}, z + \Delta z, \omega) = \frac{1}{(2\pi)^2} \int \phi(\mathbf{k}, z, \omega) e^{i\Delta z k_z(\tilde{v}(\mathbf{x}, \mathbf{k}, \omega) - \tilde{v}(\mathbf{x})) - i\mathbf{k} \cdot \mathbf{x}} d\mathbf{k}. \quad (8)$$

For $\tilde{v} = \text{constant}$, equation (7) is equivalent to the phase-screen operator (Wu and Huang, 1992), and is similar to the split-step Fourier operator of (Stoffa et al., 1990). When $\tilde{v} = v$, equation (7) is equivalent to the Fourier integral operator in equation (2). Careful selection of \tilde{v} intermediate to v and \tilde{v} provides operators that are potentially more accurate than the phase-screen operator, and much less costly to implement than the Fourier integral operator in equation (2). We will refer to the wavefield $\tilde{\Psi}$ (equation 8) as the focused wavefield, and the complex exponential in equation (7) as the differential thin-lens term.

Desample the velocity model

The Fourier transform $\mathbf{x} \rightarrow \mathbf{l}$ of equation (8) is

$$\tilde{\Phi}(\mathbf{l}, z + \Delta z, \omega) = \frac{1}{(2\pi)^2} \int_{-\infty}^{\infty} \phi(\mathbf{k}, z, \omega) \mathcal{A}(\mathbf{k}, \mathbf{l}, \omega) d\mathbf{k} d\mathbf{l}, \quad (9)$$

where

$$\mathcal{A}(\mathbf{k}, \mathbf{l}, \omega) = \int_{-\infty}^{\infty} e^{izk_z(\tilde{v}(\mathbf{x}, \mathbf{k}, \omega) - \tilde{v}(\mathbf{x}))} e^{-i\mathbf{k} \cdot \mathbf{x}} e^{i\mathbf{l} \cdot \mathbf{x}} d\mathbf{x}. \quad (10)$$

If \tilde{v} is chosen such that

$$\tilde{v}(\mathbf{x}) = (f * v)(\mathbf{x}) \quad (11)$$

where $*$ denotes convolution, and f is a high-cut filter, the number of discrete samples in the extrapolation symbol is reduced from $M \times N$, to $(m < M) \times (n < N)$ thereby reducing overall cost. Inverse Fourier transform ($\mathbf{l} \rightarrow \mathbf{x}$) completes this first alternative calculation of the focused wavefield, $\tilde{\Psi}$, of equation (8). A complete extrapolation is then accomplished by applying the differential thin-lens term with equation (7).

The cost of implementing equation (8) with the low-cut filtered version of the velocity is proportional to $mn[M \log_2 m + N \log_2 n]$ to compute \mathcal{A} , plus $MN(m+n)$ to apply \mathcal{A} , plus $MN \log_2 MN$ for the Fourier transform back to space coordinates.

PSPI plus correction

An alternative to desampling the wavefield and applying a narrow operator in the frequency domain is to reduce the number of unique velocities in the lateral coordinates. For $\tilde{v} = \lambda \times \text{round}(v/\lambda)$, where $\lambda \leq \min(v)$, the number of unique velocities p in \tilde{v} is

$$p = \frac{\max(\tilde{v}) - \min(\tilde{v})}{\lambda}. \quad (12)$$

In a procedure analogous to the PSPI method (Gazdag and Squazzerro, 1984), equation (8) becomes (Margrave and Ferguson, 1999)

$$\tilde{\Psi}(\mathbf{x}, z, \omega) = \sum_{j=1}^p \Omega(\mathbf{x}) \frac{1}{(2\pi)^2} \int \phi(\mathbf{k}, z, \omega) e^{i\Delta z k_z(v_j(\mathbf{k}, \omega) - \tilde{v}(\mathbf{x})) - i\mathbf{k} \cdot \mathbf{x}} d\mathbf{k}, \quad (13)$$

and Ω_j is a windowing function defined by

$$\Omega(\mathbf{x}) = \begin{cases} 1 & \text{if } \tilde{v}(\mathbf{x}) = v_j; \\ 0 & \text{if } \tilde{v}(\mathbf{x}) \neq v_j. \end{cases} \quad (14)$$

Unlike PSPI, no interpolation is used. The cost of implementing equation (7) with the focusing operator in equation (13) is proportional to p times the cost $MN \log_2 MN$ of the 2D FFT.

Focusing error

From Figure 1, x is the lateral distance covered by a wave incident at angle θ from the vertical when it is extrapolated distance Δz through a velocity model. The geometric relationship between x , Δz and θ is:

$$x = \Delta z \tan(\theta), \quad (15)$$

or, in terms of velocity v and slowness p

$$x = \frac{\Delta z p v}{\sqrt{1 - (p v)^2}}. \quad (16)$$

The two operators described previously achieve computational efficiency by simplifying the velocity model, and $\Delta v = v_{true} - v_{simple}$ is the resulting velocity error.

To first order, the normalized error in x as a function of v is:

$$\frac{\Delta x}{x} \approx \frac{1}{x} \frac{\partial x}{\partial v} \Delta v \approx \frac{\Delta v}{v} \frac{1}{\cos \theta}. \quad (17)$$

For a percentage error in velocity $\Delta v/v$, and a maximum desired propagation angle θ , a percentage error in focusing is given by equation (17). This percentage dictates how much the simplified velocity can deviate from the true velocity for a maximum focusing error. For the method based on desampling the velocity field, a minimum Nyquist frequency is implied. For the reduced method, a minimum number of unique velocities is implied. At every depth, the decision to use one operator over another can be made based on balancing cost and accuracy.

COMPARISONS

To compare the two operators derived above, the Marmousi model (Bourgeois et al., 1991), and the SEG/EAGE salt model (Aminzadeh et al., 1996) are used. Impulses are forward modeled by extrapolation through each velocity field to a specific time when an image of the wavefield in space is computed. Contours derived from first-arrival eikonal raytracing are plotted to provide reference. In each example, the velocity fields are simplified so each operator requires equivalent computational cost, and the resulting positioning error ($\Delta x/x$) is analyzed according to equation (17).

In 2D, the operator based on a desampled model (equation 9) computational cost c_d is given by

$$c_d = mM \log_2 m + Mm + M \log_2 M \quad (18)$$

where M is the number of inline traces and m is the number of samples in the inline direction of the velocity field. (In 2D, crossline coordinates n and N are 0 and 1 respectively.) For the operator based on the reduced model (equation 13) computational cost c_r is computed using

$$c_r = pM \log_2 M, \quad (19)$$

where p is the number of unique velocities in the lateral direction.

Marmousi

For the reduced method, the model is rounded so the result (Figure 2a) has $p = 8$ unique velocity values along the lateral coordinate and, for

$M = 512$ traces, the computational cost is proportional to $8 \times 512 \times \log_2 512 \approx 40000$ complex floating point operations.

For the desampled method, the Marmousi model is low-pass filtered so that the spatial Nyquist frequency is reduced by a factor of $16/512$ where $m = 16$. The smoothed result is given in Figure 2b. For wavefield extrapolation using equation (9), cost is proportional to $16 \times 512 \times \log_2 16 + 512 \times 16 + 512 \times \log_2 512 \approx 40000$.

In Figure 3a, the focusing errors are averaged over the lateral coordinates and plotted as functions of depth. For most depths, average error is larger for the desampled model. The greatest difference occurs at 1260m and the full velocity profile is plotted in Figure 3b. The reduced velocity tracks most of the variation in the true velocity, while the desampled velocity is a very smooth approximation. At 2020m, however, the average error associated with the reduced velocity is larger: Figure 3c shows the corresponding velocity profile and, though the reduced velocity tracks most of the true velocity, significant departures occur between 0m and 4200m distance. The desampled velocity tracks faithfully through this region, hence returns greater accuracy.

Figures 4 and 5 show comparisons of forward modeling of source impulses using the reduced method and desampled method respectively. The location of the source is distance 4670m and depth 195m, and the elapsed time is 0.82ms.

The wavefield in Figure 4 tracks the first-arrival contour more accurately than in Figure 5. Head waves should not be generated by these one-way operators and this can be seen by the absence of wave energy tracking the contour corresponding to headwaves on the left side of both Figures.

SEG salt model

For the reduced method, the model is rounded so that the reduced model (Figure 6a) has $p = 8$ (equation 19) unique velocities. For $M = 1024$ traces, the computational cost is proportional to $8 \times 1024 \times \log_2 1024 \approx 80000$ complex floating point operations.

For the desampled method, the model is low-pass filtered so that the spatial Nyquist frequency is reduced by a factor of $16/1024$ where $m = 16$. The smoothed result is given in Figure 6b. Here, the cost of the desampling method is proportional to $16 \times 1024 \times \log_2 16 + 1024 \times 16 + 1024 \times \log_2 1024 \approx 80000$.

In Figure 7a, focusing errors are averaged over the lateral coordinates and plotted as functions of depth. At levels related to the salt, average error is larger for the desampled method. Above and below the salt in the smoothly varying sediments, the desampled method returns slightly greater accuracy. Similarly, near the top of the salt at 2160m depth. The full profile is plotted in Figure 7b. The reduced velocity tracks the velocity spike corresponding to distance 6000 and poorly tracks the smooth variation of the sedimentary velocities. The desampled velocity misses the spike, but readily tracks the sediment velocity. In the salt, the average error associated with the reduced method is much less than for the desampled method in particular at 2160m depth (Figure 7).

Figures 8 and 9 show comparisons of forward modeling of source impulses using the reduced method and desampled method respectively. The location of the source is distance 6000m and depth 1000m, and the elapsed time is 0.588ms. The wavefield corresponding to the reduced method in Figure 8 tracks the first arrival contour more accurately than in Figure 9 (desampled method). Some leakage of energy from the evanescent region is visible in Figure 9 (lower right corner).

CONCLUSIONS

To reduce the cost of migration and modeling using one-way wavefield extrapolation operators, two efficient operators are derived. The first desamples the velocity model to reduce the number of significant values in the extrapolation velocity profile. The resulting computational cost is proportional to $mnMN \log_2 MN$, where M and N are the dimensions of the velocity model, and m and n are the dimensions of the

desampled velocity field. The second operator is based on a velocity model where the number of unique velocities has been reduced in the lateral direction, and is similar to the familiar PSPI plus correction method. The cost of implementing this operator is proportional to $pMN \log_2 MN$, where p is the number of unique velocities laterally.

Using the Marmousi model where velocity variation laterally is generally blocky, the reduced method returns greater accuracy for most depths.

The SEG/EAGE Salt model is laterally smooth above and below the salt body. In these regions the desampled method is slightly more accurate for equivalent computational cost. Evanescent leakage is evident in forward modeling, however, and must be dealt with prior to attempting to build a depth-migration algorithm based on a hybrid of the two operators.

ACKNOWLEDGMENTS

The authors wish to thank Dr. Sergey Fomel of the Bureau of Economic Geology, University of Texas, Austin for providing the travel-time contours used in this work.

REFERENCES

- Aminzadeh, F., Burkhard, N., Long, J., Kunz, T., and Duclos, P., 1996, Three dimensional seg/eaeg models - an update: The Leading Edge, **15**, no. 02, 131–134.
- Bourgeois, A., Bourget, M., Lailly, P., Poulet, M., Ricarte, P., and Versteeg, R., 1991, Marmousi model and data Marmousi model and data, The Marmousi experience, 5 – 9.
- Gazdag, J., and Squazzerro, P., 1984, Migration of seismic data by phase shift plus interpolation: Geophysics, **49**, 124 – 131.
- Le Rousseau, J. H., and de Hoop, M. V., 2001, Modeling and imaging with the scalar generalized-screen algorithms in isotropic media: Geophysics, **66**, 1551–1568.
- Margrave, G. F., and Ferguson, R. J., 1999, Wavefield extrapolation by nonstationary phase shift: Geophysics, **64**, 1067 – 1078.
- Stoffa, P. L., Fokkema, J. T., de Luna Freire, R. M., and Kessinger, W. P., 1990, Split-step fourier migration: Geophysics, **55**, 410–421.
- Wu, R. S., and Huang, L. Y., 1992, Scattered field calculation in heterogeneous media using phase-screen propagation: Scattered field calculation in heterogeneous media using phase-screen propagation: Soc. of Expl. Geophys., 62nd Ann. Internat. Mtg. 1289–1292.

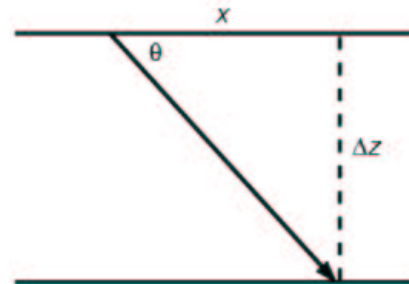


Figure 1: Illustration of a wave incident at an angle θ measured from vertical.

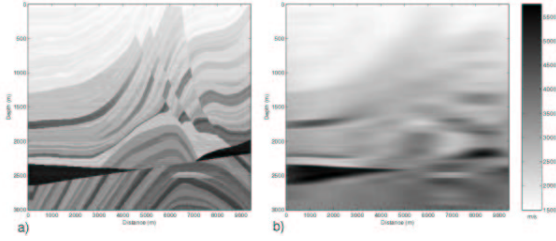


Figure 2: a) The Marmousi model reduced to 8 unique velocity values along the lateral coordinate. This velocity profile is used to generate the impulse response in Figure 4. b) The Marmousi model desampled to 16 velocity values along the lateral coordinate. This velocity profile is used to generate the impulse response in Figure 5.

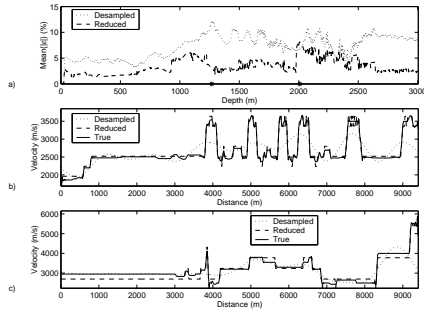


Figure 3: a) The dotted curve is the average error corresponding to the desampled velocity field of Figure 2b, and the dashed curve is the error corresponding to the reduced velocity field of Figure 2a. b) Velocity profile corresponding to 1260m depth. c) Velocity profile corresponding to 2020m depth.

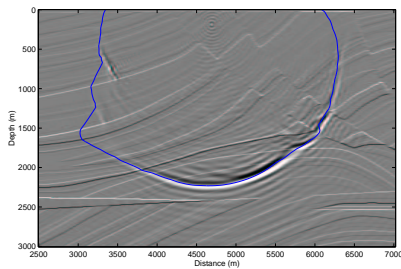


Figure 4: Snapshot of the propagating wavefield based on the reduced model of Figure 2a. The origin of the impulse is 4670m distance, and 195m depth, and the elapsed time is 0.82 seconds. The plotted line is the corresponding isochron obtained from a traveltimes calculation.

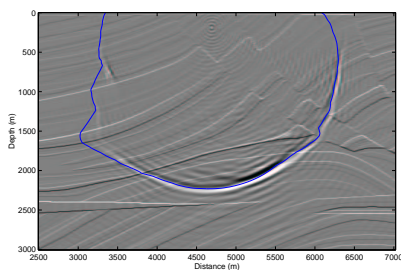


Figure 5: Snapshot of the propagating wavefield based on the reduced model of Figure 2b.

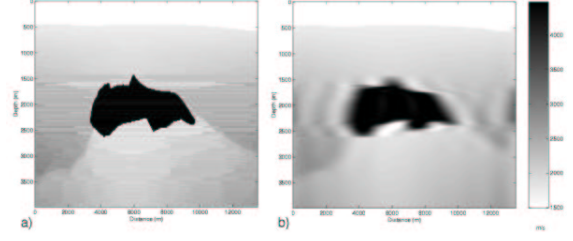


Figure 6: a) The SEG salt model reduced to 8 unique velocity values along the lateral coordinate. This velocity profile is used to generate the impulse response in Figure 8. b) The SEG salt model desampled to 16 velocity values along the lateral coordinate. This velocity profile is used to generate the impulse response in Figure 9.

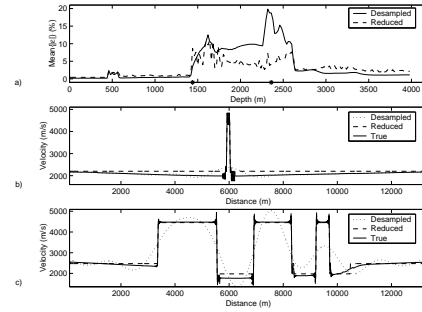


Figure 7: a) The dotted curve is the average error corresponding to the desampled velocity field of Figure 6b, and the dashed curve is the error corresponding to the reduced velocity field of Figure 6a. b) Velocity profile corresponding to 2370m depth. c) Velocity profile corresponding to 1460m depth.

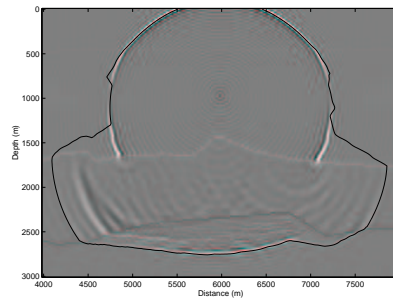


Figure 8: Snapshot of the propagating wavefield based on the reduced model of Figure 6a.

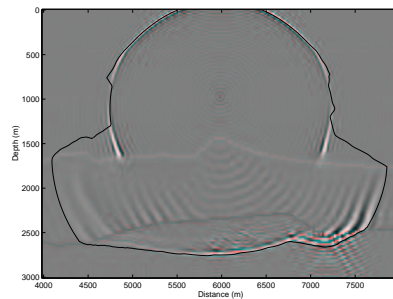


Figure 9: Snapshot of the propagating wavefield based on the desampled model of Figure 6b.